



## THERMODYNAMIC AND ENVIRONMENTAL PERFORMANCE ANALYSIS OF THE MARIB INTEGRATED POWER AND COOLING CYCLE

Abdulrazzak AKROOT<sup>1\*</sup>

<sup>1</sup>Karabük University, Faculty of Engineering, Department of Mechanical Engineering, 78050 Karabük, Türkiye

**Abstract:** Meeting energy demands while ensuring sustainability is a critical challenge in underdeveloped regions like Yemen. The Marib Integrated Power and Cooling Cycle (MIPCC) is proposed as an innovative solution to enhance power generation efficiency and reduce environmental impact by utilizing waste heat from the Marib gas turbine plant. This study evaluates the thermodynamic, economic, and environmental performance of the MIPCC system, which integrates the Brayton, Rankine, and absorption refrigeration cycles for simultaneous power generation and cooling. The results indicate that the MIPCC system significantly improves performance, achieving a net power output of 226 MW with energy and exergy efficiencies of 47.91% and 46.26%, respectively. The system reduces CO<sub>2</sub> emissions to 403.5 kg/MWh and minimizes the cost of electricity to 70.55 \$/MWh, demonstrating both environmental and economic viability. Additionally, it provides a cooling capacity of 53.5 MW, making it ideal for hot climates. The MIPCC offers a transformative energy solution by maximizing efficiency, lowering emissions, and reducing dependency on fossil fuels. Its application in energy-deprived areas can enhance energy security and economic growth, making it a scalable model for sustainable power generation in regions facing infrastructure and energy challenges.

**Keywords:** Marib power plant, Hybrid energy systems, Thermodynamic analysis, Heat recovery technology

\*Corresponding author: Karabük University, Faculty of Engineering, Department of Mechanical Engineering, 78050 Karabük, Türkiye

E mail: abdulrazzakakroot@karabuk.edu.tr (A. AKROOT)

Abdulrazzak AKROOT  <https://orcid.org/0000-0002-1561-7260>

Received: January 27, 2025

Accepted: April 05, 2025

Published: May 15, 2025

Cite as: Akroot A. 2025. Thermodynamic and environmental performance analysis of the marib integrated power and cooling cycle. BJSJ Eng Sci, 8(3): 814-823.

### 1. Introduction

Humanity is being dramatically affected by climate change, mainly caused by the consumption of fossil fuels. As per the International Energy Agency (IEA), the world's primary energy supply has increased at an average rate of 2.5% per year between 1971 and 2017, from 5519 Mtoe in 1971 to 13,972 Mtoe in 2017. According to the IEA, in 2024 alone, there were 37.34 Gt of carbon dioxide emissions. At the same time, demand for cooling has risen sharply on account of climate change and demographic trends. About 20 percent of the world's electricity is consumed for air conditioning and cooling (He et al., 2022; Wang et al., 2009).

A large amount of research has been done to develop novel thermodynamic cycles to combat the demand for decreasing fossil fuel consumption and lowering the production of greenhouse gas emissions. These advanced cycles aim to provide power and cooling simultaneously with greater efficiency than conventional, separate cycles (Kumar et al., 2010). Additionally, several of these conceptual systems utilize a low- to medium-temperature heat source, such as industrial waste heat or renewable energy, to allow for high sustainability and energy efficiency. Rostamzadeh et al. (2018) proposed a new combined cooling and power cycle that interconnected the

Kalina cycle with the ejector refrigeration cycle, also obtaining a thermal efficiency of 33.65% and cooling capacity of 160.6 kW, improving exergy efficiency and reducing irreversibility through parametric optimization. Yin et al. (2018) proposed a Goswami cycle-ejector refrigeration cycle combined cooling and power system with a thermal efficiency of 17.49% and exergy efficiency of 26.15%, whose performance was affected by absorber temperature, boiler temperature, and number of pressure stages. Parikhani et al. (2020) also designed a modified ammonia-water CCHP system based on the Kalina cycle. They obtained the energy and exergy efficiencies of 49.83% and 27.68%, respectively, and conducted a sensitivity analysis to emphasize crucial parameters (like evaporation temperature and ammonia concentration) for better performance and lower cost. Wang et al. (2019) proposed a solar thermal biomass gasification-based CCHP system achieving energy and exergy efficiencies of 56% and 28%, respectively, with a solar-to-biogas energy ratio of 0.19, showing its capability to improve biomass energy utilization significantly. Talal and Akroot (2024) evaluated a solar and Brayton cycle-based polygeneration system, achieving energy and exergy efficiencies of 51.15% and 49.4% for ISCC-ARC and 50.89% and 49.14% for ISCC, with specific costs ranging from \$69.09/MWh to



\$79.05/MWh depending on configuration and season. Aghaziarati and Aghdam (2021) introduced a solar organic Rankine cycle integrated with cascade refrigeration for hospitals, achieving energy and exergy efficiencies of 89.39% and 8.70%, respectively, with solar collectors identified as the primary source of irreversibility and cyclohexane and octane providing optimal efficiency. Wu et al. (2019) evaluated a novel CCHP system combining solar thermal and organic Rankine cycle subsystems, achieving a primary energy ratio of 60.2% and generating 108 kW, with 12.4% lower natural gas consumption compared to conventional systems. Wu et al. (2020) proposed a novel CCP system combining a regenerative sCO<sub>2</sub> Brayton cycle and ammonia-water absorption refrigeration, achieving exergy efficiency improvements of 2.29-2.54% and thermal efficiency gains of 8.16-18.93%. Nami et al. (2019) evaluated a waste-driven combined heat and power system integrated with a large-scale absorption chiller, achieving a 12% improvement in thermal efficiency, a 28.58% exergy efficiency, and an emission reduction of 445.935 kg-CO<sub>2</sub>/GJ. Salimi et al. (2022) highlighted the potential of combined cooling, heating, and power (CCHP) systems in reducing energy consumption and environmental impacts, particularly in sectors like hospitals, airports, and hydrogen production. Liao et al. (2019) proposed a novel CCHP-ORC system for recovering waste heat in coal-fired plants, achieving optimized exergy production rates using R1234ze(E) and heptane/R601a as working fluids, with parametric analysis showing a 19.4% and 18.3% decline in thermal efficiency when condenser temperature rises from 25°C to 40°C. Aghaei and Saray (2021) optimized a CCHP-Boiler system driven by a gas turbine and auxiliary boiler for a dairy factory, finding that higher air compressor pressure ratios (14.79) improve performance. At the same time, optimization reduces the need for an air pre-heater (APH), making it unnecessary. Ghorbani et al. (2023) presented a geothermal-based CCHP cogeneration system integrating Kalina, ejector refrigeration, and organic Rankine cycles, achieving an exergy efficiency of 26.55%, thermal efficiency of 23.04%, and net output power of 226 kW under optimal conditions. Chu et al. (2023) analyzed a micro-gas turbine CCHP system with an absorption chiller, achieving exergy efficiencies of 19.96% in summer and 25.13% in winter.

Despite extensive research on combined cycle systems, few studies have focused on solutions tailored for regions with energy poverty and outdated infrastructure. The Marib Integrated Power and Cooling Cycle (MIPCC) offers an innovative approach by integrating Brayton, Rankine, and absorption refrigeration cycles to enhance power and cooling efficiency under real-world constraints. This study bridges a critical gap in energy sustainability by demonstrating the economic and environmental feasibility of this hybrid system in Yemen's Marib power plant. Addressing Yemen's energy challenges, the research examines Marib's electricity shortages, exacerbated by

aging infrastructure and dependence on costly diesel generators, which hinder economic growth and daily life. The MIPCC presents a novel solution by utilizing waste heat to generate electricity, cooling, and heating, improving efficiency while lowering costs and CO<sub>2</sub> emissions. This approach transitions from conventional power generation to a more sustainable, locally adaptive model that reduces reliance on unstable energy sources. The findings provide actionable insights for addressing global energy challenges, promoting cleaner, more efficient power solutions.

## 2. Materials and Methods

### 2.1. Model Description

MIPCC is an innovative energy system which operates to improve the efficiency of power generation and effective cooling in Marib located in Yemen, as seen in Figure 1. This new cycle integrates three thermodynamic processes into one: the Brayton cycle, which is the primary cycle by which power is generated and, in this case, through gas turbines; the Rankine cycle, which accounts for further power recovery by additional steam at the expense of exhaust gases through steam turbines; and the absorption cooling cycle, which acts towards air pre-cooling (before entering the gas turbines) and the consequent help to satisfy the cooling needs. By effectively using exhaust heat and integrating these cycles, the MIPCC recovers energy economically, minimizing environmental burden and addressing sustainable energy requirements for Marib's inhospitable climate.

In the Brayton cycle, the air is compressed in the axial compressors, wherein the air is routed into the combustion chamber. Fuel is injected and mixed with air, where it burns to create high-temperature and high-pressure gases. The exhaust gases drive the gas turbines and generate mechanical power because of the heat energy of the gases. Basically, this cycle shows its primary design over power generation in a more effective way, with the use of the exhaust gases that are of significant thermal energy, which can be used in heat recovery steam generation to increase the total energy efficiency.

The Rankine Cycle absorbs the exhaust gases from the Brayton Cycle and moves them to a heat recovery steam generator (HRSG) to utilize their heat to create steam. The steam expands across three steam turbines: the High-Pressure Steam Turbine (HPST), Intermediate-Pressure Steam Turbine (IPST), and Low-Pressure Steam Turbine (LPST), which is used to drive a second generator, producing even more electricity. Once expanded, the steam is condensed as water in a condenser and pumped back into the HRSG using two open feedwater heaters (OFWH1 and OFWH2). This setup makes use of the Rankine cycle to recover energy from the exhaust gases produced by the Brayton cycle to get better power generation efficiency ultimately.

Exhaust gases from HRSG (stream 6) are used by the generator of an absorption cooling cycle that runs on a lithium bromide-water (LiBr-H<sub>2</sub>O) solution. Those

components include an absorber, solution heat exchanger (SHEX), pump (P), evaporator, and condenser. This cycle is intended primarily for pre-cooling of the air entering the Brayton cycle (stream 10a), while it also adds some additional cooling capabilities.

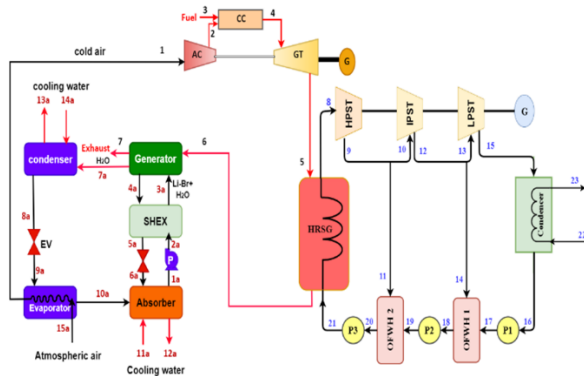


**Figure 1.** Marib integrated power and cooling cycle (MIPCC).

The Engineering Equation Solver (EES) program is used to calculate thermodynamic properties at each state point and simulate the system’s performance, ensuring accurate analysis and optimization. The simulation mode’s input parameters are presented in Table 1, and the analysis of the MIPCC system is conducted based on the following simplifying assumptions:

- All processes are considered to operate under steady-state conditions.
- Both air and flue gases are treated as ideal gas mixtures.
- Natural gas is used as the fuel in the combustion chamber.
- A constant isentropic efficiency is assumed for the compressors and the turbines, and pumps.
- The generator and evaporator outlets are assumed to produce saturated vapor water.
- The condenser outlet is assumed to yield saturated liquid.
- Pressure losses in the pipes and heat exchangers are considered negligible.
- All components are assumed to be adiabatic.
- The lithium bromide (LiBr) solutions in the generator and absorber are assumed to be in thermodynamic equilibrium with their corresponding temperatures and pressures.

While this study offers valuable insights, it has several limitations. Theoretical assumptions, including ideal gas behavior and adiabatic components, may not accurately reflect real-world inefficiencies. Methodologically, the findings rely on simulation data rather than experimental validation, underscoring the need for real-world testing and pilot studies. Furthermore, the economic feasibility assessment is based on estimated cost parameters, which are subject to fluctuations due to market dynamics, geopolitical factors, and infrastructure challenges, requiring further validation for practical implementation

**Table 1.** Input parameters for the simulation

Parameter	Value
<b>Gas Turbine Cycle</b>	
Compressor pressure ratio	11
Ambient pressure	101.3 bar
Ambient temperature	26 °C
Air mass flow rate	500 kg/s
Lower heating value of fuel	50056 kJ/kg
$\eta_{GT}$	90%
$\eta_{AC}$	86%
<b>Rankine cycle</b>	
HPST inlet pressure	100 bar
IPST inlet pressure	40 bar
LPST inlet pressure	10 bar
Condenser Temperature	40 °C
$\eta_{ST}$	90%
$\eta_{Pumps}$	85%
<b>Absorption Refrigeration Cycle</b>	
Outlet temperature of Condenser	39 °C
Evaporator temperature	5 °C
Generator temperature	88°C
Absorber temperature	37°C
Concentration of weak solution	53%
Concentration of strong solution	62%

**2.2. Thermodynamic Analysis**

The mass, energy, and exergy balance equations for each system component are expressed as follows (equations 1-3) (Noroozian et al., 2017):

$$\sum \dot{m}_{in} = \sum \dot{m}_{out} \tag{1}$$

$$\dot{Q}_{in} + \dot{W}_{in} + \sum \dot{m}_{in} h_{in} = \dot{Q}_{out} + \dot{W}_{out} + \sum \dot{m}_{out} h_{out} \tag{2}$$

$$\sum (\dot{m}ex)_{in} + \dot{E}x_Q = \sum (\dot{m}ex)_{out} + \dot{E}x_W + \dot{E}x_{des} \tag{3}$$

The subscripts “i” and “e” indicate the inlet and exit of the control volume, respectively.  $E'x_{des}$  represents the exergy destruction within each component, while “ex” corresponds to the exergy of each stream.  $\dot{E}x_W$  and  $\dot{E}x_Q$  denote the exergies associated with power and heat transfer, respectively, and are determined using the following equations 4 and 5 (El-Emam and Dincer, 2013):

$$\dot{E}x_Q = \dot{Q} \left( 1 - \frac{T_0}{T_s} \right) \tag{4}$$

$$\dot{E}x_W = \dot{W} \tag{5}$$

The energy performance denoted as  $\eta_{th}$ , can be estimated using the following equations 6 and 7:

$$\dot{W}_{net} = \dot{W}_{GT} - \dot{W}_{AC} + \dot{W}_{HPST} + \dot{W}_{LPST} + \dot{W}_{Pumps} \tag{6}$$

$$\eta_{th} = \frac{\dot{W}_{GT} - \dot{W}_{AC} + \dot{W}_{HPST} + \dot{W}_{LPST} + \dot{W}_{Pumps}}{\dot{Q}_{in}} \quad (7)$$

The heat input to the cycle ( $\dot{Q}_{in}$ ) is determined using the following equation 8:

$$\dot{Q}_{in} = \dot{m}_{fuel} \cdot LHV \cdot \eta_{CC} \quad (8)$$

Furthermore, the exergy efficiency ( $\eta_{ex}$ ) can be calculated using the given formula (equation 9), reflecting the system's effectiveness in utilizing energy quality:

$$\eta_{ex} = \frac{\dot{W}_{GT} - \dot{W}_{AC} + \dot{W}_{HPST} + \dot{W}_{LPST} + \dot{W}_{ORT} + \dot{W}_{Pumps}}{\dot{E}_3 + \dot{E}_{Q_{solar}}} \quad (9)$$

Here,  $\dot{E}_3$  denotes the exergy of the fuel supplied to the cycle's combustion chamber (CC). The rate of cooling load is determined using the following equation 10:

$$\dot{Q}_{cooling} = \dot{Q}_{Evap} - \dot{m}_1(h_{15a} - h_1) \quad (10)$$

### 2.3. Exergoeconomic and Environmental Analysis

The exergy costing process involves formulating cost balance equation 11 separately for each component of the system, as outlined below (Akroot and Al Shammre, 2024):

$$\sum(c_e \dot{E}x_e)_k + c_{w,k} \dot{W}_k = c_{Q,k} \dot{E}x_{Q,k} + \sum(c_i \dot{E}x_i)_k + \dot{Z}_k \quad (11)$$

From the above equation, it can be concluded that the cost rates of the exergy streams leaving each component are equal to the cost rates of the entering exergy streams, combined with the investment cost rate needed for the component's operation. In equation 11, "c" represents the unit cost of each exergy stream, while the capital investment cost rate,  $\dot{Z}_k$ , is calculated using equation 12 (Yang et al., 2024):

$$\dot{Z}_k = \frac{Z_k \text{CRF} \phi}{N} \quad (12)$$

In this context,  $Z_k$  represents the purchase cost of the k-th component, while  $\phi$  signifies the maintenance factor. N corresponds to the system's annual operating hours, and the Capital Recovery Factor (CRF) is calculated using

equation 13 (Nourpour et al., 2023):

$$\text{CRF} = \frac{i(1+i)^n}{(1+i)^n - 1} \quad (13)$$

The system's interest rate is set at  $i=10\%$ , with an operational lifespan of  $n=20$  years. Furthermore, the maintenance factor ( $\phi$ ) is assumed to be 1.06, and the annual operating hours (N) are specified as 2000 hours. Finally, the CO<sub>2</sub> emission rate ( $\epsilon_{CO_2}$ ) is calculated using the equation 14 provided below (Alfaris et al., 2024):

$$\epsilon_{CO_2} = \frac{\dot{m}_{CO_2}}{\dot{W}_{net}} \times 100 \quad (14)$$

### 3. Results and Discussion

Table 2 validates the results of the present study by comparing them with reference data for gas turbine and absorption refrigeration cycles, along with calculated errors. The table shows minimal errors across all parameters, indicating that the present study's results are highly consistent with reference data. The highest error is 0.92% for the exhaust temperature.

Table 3 highlights the key performance metrics of the MIPCC system, offering insights into its power generation, efficiency, and cooling capabilities. The results reveal that the system delivers a net power output of 226 MW, showcasing its ability to generate substantial power even after accounting for energy consumption by auxiliary components like pumps and compressors. With an energy efficiency of 47.91%, nearly half of the input energy is effectively converted into useful work, while the exergy efficiency of 46.26% reflects the system's effectiveness in minimizing energy losses and utilizing available resources. Additionally, the system provides a cooling capacity of 53.5 MW, underscoring its capability to deliver both power and cooling services. The coefficient of performance (COP) is 0.808, indicating how efficiently the system uses energy to produce cooling relative to its input power. The findings highlight the system's ability to balance affordability and environmental impact effectively. With a cost of 70.55 \$/MWh and CO<sub>2</sub> emissions of 403.5 kg/MWh, the system proves to be both cost-efficient and environmentally sustainable.

**Table 2.** Validation of Present Study Results with Reference Data for Gas Turbine and Absorption Refrigeration Cycle (Al-Attab, 2014; Jain et al., 2015)

Parameter	Present study	Reference	Error (%)
Gas Turbine Cycle (Al-Attab, 2014)			
Power output (MW)	163.1	163	0.06
Exhaust temperature	546	541	0.92
Exhaust mass flow	509.4	509	0.08
Efficiency	34.9	34.7	0.58
Absorption Refrigeration Cycle (Jain et al., 2015)			
Heat load in evaporator (kW)	62.15	61.63	0.84
Heat load in generator (kW)	76.78	76.98	0.26
Heat load in absorber (kW)	73.44	73.32	0.16
COP	0.752	0.749	0.4

**Table 3.** Performance Parameters of the MIPCC System

Parameter	Unit	Value
Power supplied to AC	MW	163.9
Power output of GTs	MW	320.7
Power output of HPST	MW	16.481
Power output of IPST	MW	17.795
Power output of LPST	MW	35.812
Power supplied to P1	kW	65.5
Power supplied to P2,	kW	227.6
Power supplied to P3	kW	535.7
Net power	MW	226
Overall energy efficiency	%	47.91
Overall exergy efficiency	%	46.26
Cooling capacity	MW	53.5
COP	-	0.808
CO2 emission	kg/MWh	403.5
Cost of electricity	\$/MWh	70.55

Figure 2 considers the interplay of various system parameters for the MIPCC system as the pressure ratio (PR) increases, focusing on how these changes affect the work outputs and cooling load. The findings present that the  $W_{BC}$  initially increases with rising PR, peaking around PR = 9-10 before starting to decline. At PR = 6,  $W_{BC}$  is 146.4 MW, increases to 156.8 MW at PR = 10, and then drops to 148.4 MW at PR = 18. The decline in higher PR values is attributed to the increased power consumption of the air compressor, which outweighs the gains in turbine work output. The  $W_{RC}$  decreases steadily as the PR increases, dropping from 98.35 MW at PR = 6 to 50.37 MW at PR = 18. This decline is directly linked to the reduction in the turbine exhaust temperature ( $T_5$ ), which feeds the HRSG. The lower  $T_5$  results in reduced heat transfer to the HRSG, thereby limiting the work output of the Rankine cycle. The  $W_{net}$  is the sum of the Brayton and Rankine cycles, reflecting the combined contributions of both cycles. As the PR increases,  $W_{net}$  decreases from 244.8 MW at PR = 6 to 198.7 MW at PR = 18. This reduction is primarily caused by two factors: the increased power consumption of the air compressor at higher PR values, which reduces  $W_{BC}$ , and the steady decline in  $W_{RC}$  due to lower thermal energy entering the HRSG, driven by a decrease in turbine exhaust temperature. The cooling load ( $Q_{cooling}$ ) decreases steadily as the PR increases, dropping from 57.46 MW at PR = 6 to 50.2 MW at PR = 18. This reduction is directly linked to the decline in  $T_6$ . As  $T_6$  decreases, the generator's heat energy is reduced, lowering the cooling load, as less energy needs to be dissipated. The rate of decrease is more gradual at lower PR values (PR = 6-10) but becomes more pronounced at higher PR values (PR = 11-18), indicating a stronger influence of reduced thermal input at elevated PR levels. This aligns with the reduction in turbine exhaust temperature ( $T_5$ ).

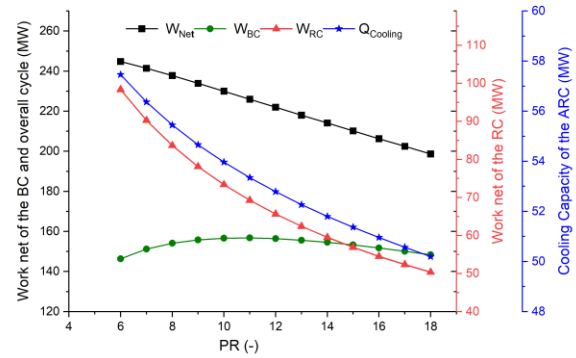
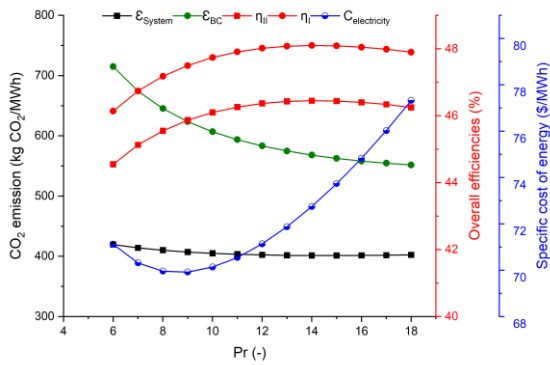


**Figure 2.** Variation of work net and Cooling Load with Pressure Ratio (PR) in the MIPCC System.

Figure 3 provides insights into the performance of the MIPCC system, focusing on key parameters such as CO<sub>2</sub> emissions ( $\epsilon_{system}$  and  $\epsilon_{BC}$ ), efficiencies ( $\eta_I$  and  $\eta_{II}$ ), and the specific cost of energy ( $C_{electricity}$ ). The results indicate that the reduction in CO<sub>2</sub> emissions in the MIPCC system is primarily driven by two factors: the contribution of the Rankine cycle, which recovers waste heat from the Brayton cycle's exhaust, and the cooling of ambient air before it enters the Brayton cycle. This pre-cooling process enhances Brayton cycle efficiency, reduces fuel consumption, and lowers emissions. CO<sub>2</sub> emissions for the MIPCC system decrease steadily with increasing PR, from 419.6 kg CO<sub>2</sub>/MWh at PR = 6 to 402.5 kg CO<sub>2</sub>/MWh at PR = 18. Compared to the standalone Brayton cycle, the MIPCC system achieves significant emission reductions, with the Rankine cycle and cooling mechanisms playing essential roles in optimizing fuel utilization and overall environmental performance. At lower PR values (PR = 6-9), emissions decrease more substantially, reaching up to 41.3%, due to greater waste heat recovery and a more pronounced cooling effect. However, at higher PR values (PR > 12), the percentage drops to 27.1% as the Brayton cycle's inherent efficiency improves, reducing the relative impact of the Rankine cycle and cooling.

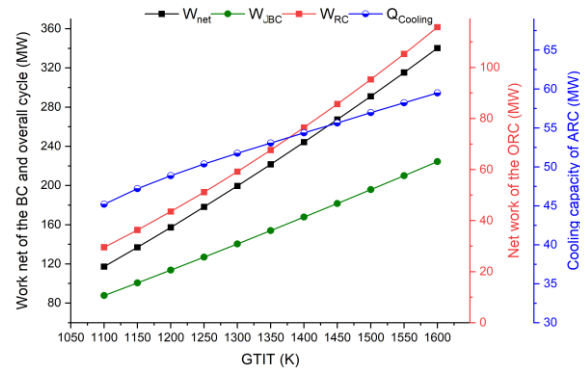
The overall efficiencies of the MIPCC system, represented by the first-law efficiency ( $\eta_I$ ) and second-law (exergy) efficiency ( $\eta_{II}$ ), are crucial for evaluating the system's thermodynamic performance. At lower pressure ratios (PR = 6),  $\eta_I$  is 44.55%, benefiting from improved heat transfer and reduced irreversibilities. As PR increases,  $\eta_I$  reaches a peak of 46.48% at PR = 12 due to the balanced contributions of the Brayton and Rankine cycles, which optimize thermal energy utilization and work output. However, at higher PR values (PR > 12), increased compressor work reduces the fraction of input energy converted into useful work, causing  $\eta_I$  to decline slightly to 46.25% at PR = 18. The second-law efficiency ( $\eta_{II}$ ) follows a similar trend, starting at 46.14% at PR = 6 and peaking at 48.08% at PR = 12, primarily due to the Rankine cycle's role in recovering waste heat and minimizing irreversibilities. At higher PR values (PR > 12),  $\eta_{II}$  decreases slightly to 47.9%, as exergy destruction becomes more significant in components like the compressor and heat exchangers. The PR range of 9-12 is

identified as the optimal operating range, balancing the contributions of the Brayton and Rankine cycles while maintaining high efficiency and minimizing losses. The specific cost of energy ( $C_{\text{electricity}}$ ) in the MIPCC system shows a distinct trend: it decreases initially with increasing pressure ratio (PR), reaching a minimum of 69.92 \$/MWh at PR = 9, and then rises steadily to 77.33 \$/MWh at PR = 18. The system operates less efficiently at low PR values due to lower Brayton cycle efficiency and limited energy recovery from the Rankine cycle, resulting in higher energy costs. The system achieves optimal performance at moderate PR values (PR = 9-12), with high thermal efficiency ( $\eta_I$ ) and effective waste heat recovery, minimizing  $C_{\text{electricity}}$ . However, at high PR values (PR = 13-18), the specific cost increases due to higher compressor power consumption, reduced contributions from the Rankine cycle caused by lower turbine exhaust temperatures, and increased system irreversibilities. To minimize  $C_{\text{electricity}}$ , the system should operate within the optimal PR range of 9-12, enhance the Rankine cycle's heat recovery capabilities, and reduce compressor irreversibilities.



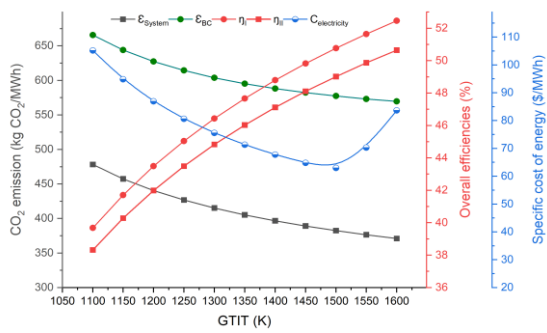
**Figure 3.** Impact of pressure ratio (PR) on CO<sub>2</sub> emissions, overall efficiencies, and specific cost of energy for the MIPCC system.

Figure 4 highlights the influence of varying gas turbine inlet temperature (GTIT) on the MIPCC system performance metrics. The results reflect significant trends in the network ( $W_{\text{net}}$ ), Brayton cycle work ( $W_{\text{BC}}$ ), Rankine cycle work ( $W_{\text{RC}}$ ), and cooling load ( $Q_{\text{cooling}}$ ). The findings reveal that increasing GTIT enhances overall system performance by boosting work outputs from both the Brayton and Rankine cycles while providing higher cooling capacity. As the GTIT increases, the  $W_{\text{net}}$  improves significantly, rising from 117.4 MW at GTIT=1100K to 315.2 MW at GTIT=1600K. This enhancement is driven by the greater energy supplied to the gas turbine, boosting  $W_{\text{BC}}$ , which increases from 87.73 MW to 224.5 MW. Simultaneously, the  $W_{\text{RC}}$  exhibits consistent growth, rising from 29.71 MW to 115.5 MW, as the elevated GTIT increases the exhaust temperature and heat energy supplied to the HRSG. The  $Q_{\text{cooling}}$  grows with  $T_4$ , ranging from 45.21 MW to 59.5 MW.



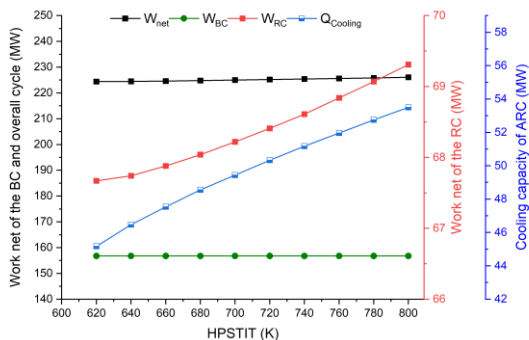
**Figure 4.** Effect of Gas Turbine Inlet Temperature (GTIT) on Work Outputs and Cooling Capacity in the MIPCC System.

Figure 5 demonstrates that increasing GTIT enhances the performance of the MIPCC system across key metrics, including efficiencies, emissions, and economic cost. Operating within the GTIT range of 1450-1500 K achieves the best balance between thermodynamic efficiency, environmental sustainability, and economic viability. The results showed that the MIPCC system's lower CO<sub>2</sub> emissions are a direct result of the Rankine cycle's ability to utilize waste heat and the additional contribution of the absorption cycle. Together, these processes reduce the amount of exhaust gases released into the atmosphere, significantly improving efficiency and reducing environmental impact. Without these integrations, the exhaust from the Brayton cycle would result in higher direct emissions. The system's emissions ( $\epsilon_{\text{system}}$ ) steadily decrease as GTIT increases, dropping from 478.2 kg CO<sub>2</sub>/MWh at GTIT = 1100 K to 371 kg CO<sub>2</sub>/MWh at GTIT = 1600 K. In comparison, the Brayton cycle's emissions ( $\epsilon_{\text{BC}}$ ) are consistently higher, decreasing from 665.6 kg CO<sub>2</sub>/MWh at GTIT = 1100 K to 569.6 kg CO<sub>2</sub>/MWh at GTIT = 1600 K. These trends demonstrate superior efficiency and reduce the environmental impact of the MIPCC system compared to the standalone Brayton cycle, as the integration of the Rankine cycle enables better utilization of waste heat and reduced fuel consumption. The system's second-law efficiency ( $\eta_{II}$ ) increases with the GTIT, rising from 38.32% at GTIT = 1100 K to 50.56% at GTIT = 1600 K. This improvement reflects reduced irreversibilities, particularly in the HRSG and Rankine cycle, as waste heat from the Brayton cycle is effectively converted into additional work, minimizing exergy destruction. Similarly, the first-law efficiency ( $\eta_I$ ) also rises, from 39.68% at GTIT = 1100 K to 52.46% at GTIT = 1600 K. Enhanced thermal efficiency ensures less energy is wasted as heat, requiring less fuel for the same energy output. The specific cost of energy ( $C_{\text{electricity}}$ ) decreases initially as the gas turbine inlet temperature (GTIT) increases, reaching its lowest value of 63 \$/MWh at GTIT = 1450 K. However, at higher GTIT values, it begins to rise slightly. This trend is influenced by increased operational and maintenance demands, as well as greater thermal stress and exergy destruction at elevated GTIT levels, resulting in a higher cost per unit of energy.



**Figure 5.** Impact of gas turbine inlet temperature (GTIT) on CO<sub>2</sub> emissions, overall efficiencies, and specific cost of energy for the MIPCC system.

Figure 6 illustrates the effect of HPSTIT (High-Pressure Steam Turbine Inlet Temperature) on key performance metrics of the MIPCC system, including the Brayton Cycle work ( $W_{BC}$ ), Rankine Cycle work ( $W_{RC}$ ), network ( $W_{net}$ ), and cooling capacity ( $Q_{cooling}$ ). The results show that the  $W_{BC}$  remains constant at 156.8 MW across all HPSTITs, as it is independent of the inlet temperature and primarily relies on turbine and compressor performance. In contrast, the  $W_{RC}$  decreases slightly as HPSTIT drops, declining from 69.31 MW at HPSTIT = 800 K to 67.67 MW at HPSTIT = 620 K. This reduction occurs because lower HPSTIT reduces the thermal energy supplied to the high-pressure steam turbine, resulting in diminished heat recovery from the HRSG and, consequently, lower power generation in the Rankine cycle.  $W_{net}$  slightly decreases from 226.1 MW at HPSTIT = 800 K to 224.4 MW at HPSTIT = 620 K. The combined contributions of the Brayton and Rankine cycles influence the network. Since  $W_{BC}$  remains constant, the decrease in  $W_{net}$  is directly linked to the reduction in  $W_{RC}$  as HPSTIT decreases. The  $Q_{cooling}$  decreases consistently as HPSTIT decreases, dropping from 53.5 MW at HPSTIT = 800 K to 45.17 MW at HPSTIT = 620 K. When HPSTIT increases, the generator inlet temperature rises, leading to greater heat input to the generator and a higher cooling load. Conversely, a lower HPSTIT reduces the thermal energy supplied to the generator, resulting in a decreased cooling load.



**Figure 6.** Effect of HPSTIT (High-Pressure Steam Turbine Inlet Temperature) on Work Outputs and Cooling Capacity in the MIPCC System.

Figure 7 shows how the HPSTIT influences the key performance metrics of the MIPCC system, such as CO<sub>2</sub> emissions ( $\epsilon_{system}$  and  $\epsilon_{BC}$ ), first-law efficiency ( $\eta_I$ ), second-

law efficiency ( $\eta_{II}$ ), specific cost of energy ( $C_{electricity}$ ). The results present a slight increase in the system's CO<sub>2</sub> emissions ( $\epsilon_{system}$ ) as HPSTIT decreases primarily due to the reduced performance of the Rankine cycle in recovering waste heat from the Brayton cycle exhaust. At higher HPSTIT values, the Rankine cycle operates more efficiently because the higher inlet temperature provides greater thermal energy for steam expansion in the turbine, enabling the Rankine cycle to generate more work. This reduces CO<sub>2</sub> emissions. As HPSTIT decreases, the thermal energy available for the Rankine cycle diminishes, resulting in less work being produced. This forces the system to rely more heavily on the Brayton cycle to meet the required power output. Since the Brayton cycle has higher specific CO<sub>2</sub> emissions and operates independently of HPSTIT, the overall system's CO<sub>2</sub> emissions increase slightly due to the reduced contribution from the Rankine cycle. In contrast, the Brayton cycle's CO<sub>2</sub> emissions ( $\epsilon_{BC}$ ) remain constant at 593.8 kg CO<sub>2</sub>/MWh because the Brayton cycle's fuel consumption is independent of the HPSTIT and solely depends on its own thermodynamic conditions, such as the gas turbine inlet temperature and compressor work. The second-law efficiency ( $\eta_{II}$ ) decreases slightly as the HPSTIT decreases, ranging from 46.27% at HPSTIT = 800 K to 45.93% at HPSTIT = 620 K. At higher HPSTIT, the Rankine cycle has greater thermal energy input, enabling it to recover more waste heat from the Brayton cycle's exhaust. This leads to more efficient conversion of thermal energy into work, reducing irreversibilities and improving  $\eta_{II}$ . As HPSTIT decreases, the thermal energy entering the high-pressure steam turbine is reduced, limiting the Rankine cycle's ability to recover waste heat effectively. This increases the relative irreversibilities in the system, causing a slight decline in  $\eta_{II}$ . Similarly, the first-law efficiency ( $\eta_I$ ) marginally decreases, from 47.92% at HPSTIT = 800 K to 47.57% at HPSTIT = 620 K, as the reduced thermal energy supplied to the steam turbine limits its power generation capacity, slightly lowering the overall efficiency of the system. The specific cost of energy ( $C_{electricity}$ ) increases as the HPSTIT decreases, rising from 70.49 \$/MWh at HPSTIT = 800 K to 73.31 \$/MWh at HPSTIT = 620 K. This trend is driven by the reduced contribution of the Rankine cycle to the overall power output at lower HPSTIT, which raises the specific cost of energy.

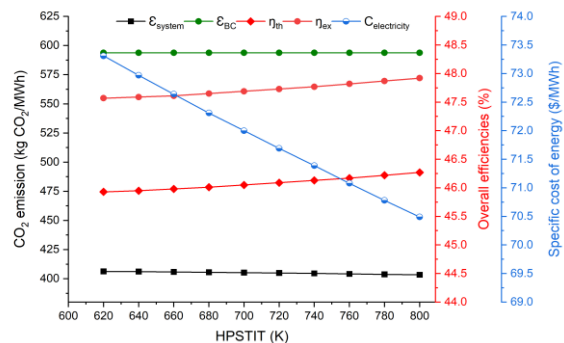


**Figure 7.** Effect of high-pressure steam turbine inlet temperature (HPSTIT) on system efficiency, CO<sub>2</sub> emissions, and specific energy cost in the MIPCC system.

Figure 8 demonstrates how the HPSTIP (High-Pressure Steam Turbine Inlet Pressure) affects the work output and cooling capacity in the MIPCC system. The findings reveal that the  $W_{BC}$  remains constant at 156.8 MW across all HPSTIP, as its performance is unaffected by changes in HPSTIP, being determined solely by the gas turbine and compressor. In contrast, the  $W_{RC}$  steadily increases with higher HPSTIP, rising from 64.36 MW at 60 bar to 72.63 MW at 150 bar. This improvement is due to enhanced thermodynamic efficiency in the Rankine cycle, as the higher pressure allows steam to expand more effectively in the turbine, generating greater output and contributing significantly to overall system performance. Consequently, the  $W_{net}$  of the system also increases with HPSTIP, growing from 221.1 MW at 60 bar to 229.4 MW at 150 bar, reflecting the direct impact of the Rankine cycle's enhanced output. Conversely, the cooling capacity ( $Q_{cooling}$ ) decreases with increasing HPSTIP, from 56.18 MW at 60 bar to 51.2 MW at 150 bar, as higher HPSTIP leads to more efficient energy conversion in the Rankine cycle, reducing the amount of heat that needs to be rejected as waste, and lowering the heat enters to the generator.

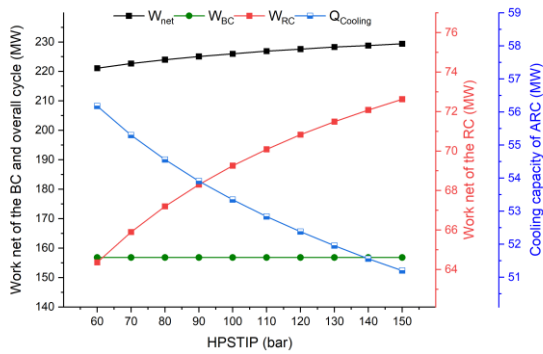


**Figure 8.** Effect of HPSTIP (High-pressure steam turbine inlet pressure) on work outputs and cooling capacity in the MIPCC system.

Figure 9 illustrates how variations in HPSTIP impact key performance metrics of the MIPCC power plant, including CO<sub>2</sub> emissions ( $\epsilon_{system}$  and  $\epsilon_{BC}$ ), system efficiencies ( $\eta_{II}$  and  $\eta_I$ ), and the specific cost of energy ( $C_{electricity}$ ). The system's CO<sub>2</sub> emissions decrease as HPSTIP increases, from 412.3 kg CO<sub>2</sub>/MWh at HPSTIP = 60 bar to 397.7 kg CO<sub>2</sub>/MWh at HPSTIP = 150 bar. As HPSTIP increases, the Rankine cycle becomes more efficient due to improved steam expansion in the turbine. This allows the system to recover more waste heat and generate more power without additional fuel consumption, reducing CO<sub>2</sub> emissions per unit of energy produced.  $\epsilon_{BC}$  remains constant at 593.8 kg CO<sub>2</sub>/MWh across all HPSTIP values. The Brayton cycle's emissions are solely determined by its fuel consumption, which is unaffected by changes in HPSTIP.  $\eta_{II}$  improves steadily from 45.26% at HPSTIP = 60 bar to 46.95% at HPSTIP = 150 bar. The second-law efficiency reflects the system's ability to minimize irreversibilities and effectively utilize available exergy. Higher HPSTIP enhances steam expansion in the turbine, improving

energy recovery in the Rankine cycle and reducing exergy losses. This leads to a gradual improvement in  $\eta_{II}$ .  $\eta_I$  increases from 46.87% at HPSTIP = 60 bar to 48.62% at HPSTIP = 150 bar. Higher HPSTIP improves the thermodynamic performance of the Rankine cycle, increasing its contribution to the total work output and enhancing the system's overall thermal efficiency.  $C_{electricity}$  decreases from 73.28 \$/MWh at HPSTIP = 60 bar to 68.81 \$/MWh at HPSTIP = 150 bar. As HPSTIP increases, the Rankine cycle generates more power due to better energy recovery from the steam turbine. This reduces operational costs, resulting in a lower specific cost of energy.

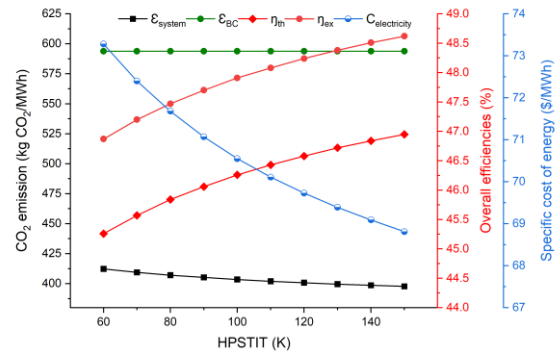


**Figure 9.** Effect of high-pressure steam turbine inlet pressure (HPSTIP) on system efficiency, CO<sub>2</sub> emissions, and specific energy cost in the MIPCC system.

### 6. Conclusion

This study addresses Yemen's pressing energy challenges by investigating the Marib integrated power and cooling cycle (MIPCC), centered around the Marib power plant, as a potential future solution. The proposed system enhances power generation and cooling efficiency by utilizing waste heat from the gas turbine exhaust. Using a simulation-based approach, the system's performance was validated against reference data, with cooling loads and efficiencies systematically evaluated to ensure optimal performance. The main findings of the study are as follows:

- The MIPCC system makes efficient use of waste heat, leading to a 47.91% improvement in energy efficiency and a 46.26% boost in exergy efficiency compared to standalone systems.
- CO<sub>2</sub> emissions were significantly reduced to 403.5 kg/MWh, and the specific cost of electricity dropped to 70.55 \$/MWh, demonstrating the system's environmental and economic benefits.
- The system provides a cooling capacity of 53.5 MW with a COP of 0.808, ensuring reliable cooling performance even under harsh conditions.
- The Rankine cycle's use of waste heat proved to be a key driver for improving efficiency and power output, outperforming other standalone configurations.
- Compared to traditional setups, the MIPCC system achieved lower emissions, and higher

power generation, making it a more sustainable and efficient option.

- The economic analysis showed a promising payback period, confirming the system's viability as a practical solution to Yemen's energy shortages.

Overall, the MIPCC system provides a sustainable, efficient, and cost-effective solution for enhancing energy stability in regions with similar challenges. Future research should focus on experimental validation to confirm simulation results, optimizing thermodynamic and economic performance for large-scale deployment, and integrating renewable energy sources like solar or biomass to improve sustainability. Additionally, a comprehensive techno-economic assessment across diverse geographical locations with varying climates and resource availability will be crucial for broader applicability and long-term feasibility.

**Author Contributions**

The percentages of the author' contributions are presented below. The author reviewed and approved the final version of the manuscript.

	A.A.
C	100
D	100
S	100
DCP	100
DAI	100
L	100
W	100
CR	100
SR	100
PM	100
FA	100

C=Concept, D=design, S=supervision, DCP=data collection and/or processing, DAI=data analysis and/or interpretation, L=literature search, W=writing, CR=critical review, SR=submission and revision, PM=project management, FA= funding acquisition.

**Conflict of Interest**

The author declares no conflict of interest.

**Ethical Consideration**

Ethics committee approval was not required for this study because of there was no study on animals or humans.

**References**

Aghaei AT, Saray RK. 2021. Optimization of a combined cooling, heating, and power (CCHP) system with a gas turbine prime mover: A case study in the dairy industry. *Energy* 229: 120788. <https://doi.org/10.1016/j.ENERGY.2021.120788>.

Aghaziarati Z, Aghdam AH. 2021. Thermoeconomic analysis of a novel combined cooling, heating and power system based on solar organic Rankine cycle and cascade refrigeration cycle. *Renew Energy* 164: 1267-1283.

<https://doi.org/10.1016/j.RENENE.2020.10.106>.

Akroot A, Al Shammre AS. 2024. Techno-Economic and Environmental Impact Analysis of a 50 MW Solar-Powered Rankine Cycle System. *Processes* 12: 1059. <https://doi.org/10.3390/pr12061059>.

Al-Attab K. 2014. Enhancement of Marib Gas Turbine Power Station Using Recuperator. *J Eng Sci* 3: 80-94.

Alfaris A, Akroot A, Deniz E. 2024. The Exergo-Economic and Environmental Evaluation of a Hybrid Solar-Natural Gas Power System in Kirkuk. *Appl Sci* 14: 10113. <https://doi.org/10.3390/app142210113>.

Chu S, Zhang H, Chen H. 2023. Energy, exergy, energy-saving, economic and environmental analysis of a micro-gas turbine-PV/T combined cooling, heating and power (CCHP) system under different operation strategies: Transient simulation. *Energy Convers Manag* 276: 116557. <https://doi.org/10.1016/j.ENERGY.2022.116557>.

El-Emam RS, Dincer I. 2013. Exergy and exergoeconomic analyses and optimization of geothermal organic Rankine cycle. *Appl Therm Eng* 59: 435-444. <https://doi.org/10.1016/j.applthermaleng.2013.06.005>.

Ghorbani S, Deymi-Dashtebayaz M, Dadpour D, Delpisheh M. 2023. Parametric study and optimization of a novel geothermal-driven combined cooling, heating, and power (CCHP) system. *Energy* 263: 126143. <https://doi.org/10.1016/j.ENERGY.2022.126143>.

He X, Li CC, Wang H. 2022. Thermodynamics analysis of a combined cooling, heating and power system integrating compressed air energy storage and gas-steam combined cycle. *Energy* 260: 125105. <https://doi.org/10.1016/j.ENERGY.2022.125105>.

Jain V, Sachdeva G, Kachhwaha SS. 2015. Energy, exergy, economic and environmental (4E) analyses based comparative performance study and optimization of vapor compression-absorption integrated refrigeration system. *Energy* 91: 816-832. <https://doi.org/10.1016/j.ENERGY.2015.08.041>.

Kumar A, Kumar K, Kaushik N, Sharma S, Mishra S. 2010. Renewable energy in India: Current status and future potentials. *Renew Sustain Energy Rev* 14: 2434-2442. <https://doi.org/10.1016/j.RSER.2010.04.003>.

Liao G, Liu L, Zhang F, Jiaqiang E, Chen J. 2019. A novel combined cooling-heating and power (CCHP) system integrated organic Rankine cycle for waste heat recovery of bottom slag in coal-fired plants. *Energy Convers Manag* 186: 380-392. <https://doi.org/10.1016/j.ENERGY.2019.02.072>.

Nami H, Arabkoohsar A, Anvari-Moghaddam A. 2019. Thermodynamic and sustainability analysis of a municipal waste-driven combined cooling, heating and power (CCHP) plant. *Energy Convers Manag* 201: 112158. <https://doi.org/10.1016/j.ENERGY.2019.112158>.

Noroozian A, Mohammadi A, Bidi M, Ahmadi MH. 2017. Energy, exergy and economic analyses of a novel system to recover waste heat and water in steam power plants. *Energy Convers Manag* 144: 351-360. <https://doi.org/10.1016/j.ENERGY.2017.04.067>.

Nourpour M, Khoshgoftar Manesh MH, Pirozfar A, Delpisheh M. 2023. Exergy, Exergoeconomic, Exergoenvironmental, Energy-based Assessment and Advanced Exergy-based Analysis of an Integrated Solar Combined Cycle Power Plant. *Energy Environ* 34: 379-406. <https://doi.org/10.1177/0958305X211063558>.

Parikhani T, Azariyan H, Behrad R, Ghaebi H, Jannatkah J. 2020. Thermodynamic and thermoeconomic analysis of a novel ammonia-water mixture combined cooling, heating, and power (CCHP) cycle. *Renew Energy* 145: 1158-1175.

- Rostamzadeh H, Ghaebi H, Parikhani T. 2018. Thermodynamic and thermoeconomic analysis of a novel combined cooling and power (CCP) cycle. *Appl Therm Eng* 139: 474-487. <https://doi.org/10.1016/J.APPLTHERMALENG.2018.05.001>.
- Salimi M, Hosseinpour M, Mansouri S, Borhani TN. 2022. Environmental aspects of the combined cooling, heating, and power (CCHP) systems: a review. *Processes* 10: 711.
- Talal W, Akroot A. 2024. An Exergoeconomic Evaluation of an Innovative Polygeneration System Using a Solar-Driven Rankine Cycle Integrated with the Al-Qayyara Gas Turbine Power Plant and the Absorption Refrigeration Cycle. *Machines* 12: 133. <https://doi.org/10.3390/machines12020133>.
- Wang J, Dai Y, Sun Z. 2009. A theoretical study on a novel combined power and ejector refrigeration cycle. *Int J Refrig* 32: 1186-1194. <https://doi.org/10.1016/J.IJREFRIG.2009.01.021>.
- Wang J, Ma C, Wu J. 2019. Thermodynamic analysis of a combined cooling, heating and power system based on solar thermal biomass gasification. *Appl Energy* 247: 102-115. <https://doi.org/10.1016/J.APENERGY.2019.04.039>.
- Wu C, Xu X, Li Q, Li J, Wang S, Liu C. 2020. Proposal and assessment of a combined cooling and power system based on the regenerative supercritical carbon dioxide Brayton cycle integrated with an absorption refrigeration cycle for engine waste heat recovery. *Energy Convers Manag* 207: 112527. <https://doi.org/10.1016/J.ENCONMAN.2020.112527>.
- Wu D, Zuo J, Liu Z, Han Z, Zhang Y, Wang Q. 2019. Thermodynamic analyses and optimization of a novel CCHP system integrated organic Rankine cycle and solar thermal utilization. *Energy Convers Manag* 196: 453-466. <https://doi.org/10.1016/J.ENCONMAN.2019.06.020>.
- Yang K, He Y, Du N, Yan P, Zhu N, Chen Y. 2024. Exergy, exergoeconomic, and exergoenvironmental analyses of novel solar- and biomass-driven trigeneration system integrated with organic Rankine cycle. *Energy* 301: 364-378. <https://doi.org/10.1016/j.energy.2024.131605>.
- Yin J, Yu Z, Zhang C, Tian M, Han J. 2018. Thermodynamic analysis of a novel combined cooling and power system driven by low-grade heat sources. *Energy* 156: 319-327. <https://doi.org/10.1016/J.ENERGY.2018.05.070>.